Supplementary Materials for

Authigenic origin of a Shuram-like excursion

Lei Jiang, Noah Planavsky, Mingyu Zhao, Wei Liu, and Xiangli Wang

1. Materials and Methods

Thin sections were prepared and stained using Alizarin Red S to differentiate calcite from dolomite in all samples (Dickson, 1966). Samples collected for this study were collected from repetitive, laterally persistent beds of evaporite, dolomicrite, with minor interbeded organic matter and magnesite, and overlain by dolostone and limestone. All thin sections were examined by transmitted-light microscopy, and selected samples were prepared for scanning electron microscope (SEM), carbon and oxygen, and strontium isotopic analyses.

Organic and Carbonate Carbon and Oxygen Isotopes

Powder samples (30–50 mg per single sample) of limestone, dolostone, and carbonate cements were collected for carbon and oxygen isotopic measurements. The powered samples were roasted at 60°C for 13 h and at 110 °C for 3 h to remove organic material, and then they were reacted with anhydrous phosphoric acid, under vacuum, to release CO_2 at 25 °C for 24 h. CO_2 was then analyzed for carbon and oxygen isotopes on a Finnigan MAT251 or Delta-V mass spectrometer. All carbon and oxygen data are reported in ‰ units relative to the Vienna Pee Dee Belemnite (VPDB) standard. The precision for both $\delta^{13}C$ and $\delta^{18}O$ measurements is better than ±0.1‰ based on within run geostandard measurements. Organic carbon samples were analyzed at Yale University using a Costech ESC 4010 Elemental Combustion System (Costech Analytical Technologies, Valencia, CA, USA) interfaced with a

Thermo Delta Plus Advantage isotope ratio mass spectrometer (Thermo, Bremen, Germany).

Carbonate Uranium Isotope

Powders were leached in 0.5-molar acetic acid at room temperature for 4 h and 3.4-molar acetic acid at 60°C for 24 h, respectively. Trace elements were measured at Yale University from splits from each digest on a ThemoFinnigan Element XR magnetic sector ICP-MS. Element measurement precision was better than 5% for duplicate samples. For U isotopes, the ^{236}U-^{233}U double spike was added and samples were prepared using the UTEVA column method similar to Wang et al. (2016) and Hood et al. (2018). $^{238}U/^{235}U$ is measured on a ThemoFinnigan NeptunePlus multi-collector ICP-MS at Yale University at low mass resolution, with a blank U level <50 pg. $^{238}U/^{235}U$ values are reported relatively to CRM-112a (0.0‰). External reproducibility was better than 0.07‰ (2SD) based on full protocol duplicates of the geostandard NOD-A-1.

Carbonate Strontium Isotope

Fine powder samples were obtained using a low-speed microdrill and then analyzed for strontium, carbon, and oxygen isotopic data. Calcite and dolomite samples were leached in 0.5-molar acetic acid at room temperature for 4 h and 3.4 molar acetic acid at 60°C for 24 h, respectively. The strontium was further separated by conventional cation-exchange techniques using ion-exchange resin (packed with Bio-Rad AG50Wx8). Strontium isotopic analyses were performed on a Finnigan MAT-262 multicollector thermal ionization mass spectrometer (TIMS) at the Institute of Geology and Geophysics, Chinese Academy of Sciences. The measured values for the

NBS-987 standard were $^{87}Sr/^{86}Sr$: 0.710265 ±0.000013 (n = 8, 1 SD). Over the whole procedure, the Sr blank was lower than 300 pg.

2. Table S1

$\delta^{13}C$, $\delta^{18}O$, $\delta^{238}U$, and $^{87}Sr/^{86}Sr$ values from the Lower Triassic Leikoupo Formation in the Sichuan Basin, China

Sample No.	Depth (m)	Lithology	$\delta^{13}C_{carb}$ (‰)	$\delta^{18}O_{carb}$ (‰)	$\delta^{13}C_{org}$ (‰)	$\delta^{238}U_{carb}$ (‰)	2SE (‰)	$^{87}Sr/^{86}Sr$
G-01	3043.00	Limestone	5.6	-4.7	--	--	--	--
G-02	3044.08	Limestone	5.9	-2.7	--	--	--	0.708179
G-03	3045.10	Limestone	5.9	-2.7	--	--	--	--
G-04	3046.60	Limestone	5.4	-4.3	--	--	--	--
G-05	3046.51	Limestone	5.9	-2.8	--	--	--	0.708235
G-06	3047.44	Limestone	5.5	-3	-26.0	--	--	--
G-07	3048.45	Limestone	5.5	-3.2	--	--	--	--
G-08	3049.16	Limestone	5.4	-5	--	--	--	0.708277
G-09	3050.41	Limestone	5.4	-5.3	--	--	--	--
G-10	3051.50	Limestone	5	-5.5	--	--	--	0.708235
G-11	3052.07	Dolostone	5.3	-3.8	--	--	--	--
G-12	3053.03	Dolostone	--	--	--	--	--	0.708288
G-13	3054.32	Dolostone	4.9	-0.8	--	-0.30	0.05	--
G-14	3054.85	Dolostone	4.6	-0.4	-27.7	-0.35	0.09	--
G-15	3055.31	Dolostone	4.4	-1.2	--	-0.49	0.06	--
G-16	3056.70	Dolomite	4.4	1.2	--	--	--	--
G-17	3057.14	Dolostone	4.8	-0.4	--	--	--	0.708430
G-18	3058.90	Carb&Eva	0.5	0.1	-28.0	-0.56	0.07	--
G-19	3059.37	Carb&Eva	-1.6	-3.7	--	--	--	--
G-20	3059.78	Carb&Eva	2.1	-1.2	--	--	--	--
G-21	3060.25	Carb&Eva	-1.3	-2.4	-27.4	-0.33	0.04	0.708298
G-22	3061.46	Carb&Eva	-1.9	0.3	--	--	--	--
G-23	3062.04	Carb&Eva	-1.7	0.7	-26.8	-0.50	0.05	--
G-24	3063.72	Carb&Eva	-5.2	-3.7	--	--	--	--

G-25	3065.04	Carb&Eva	-8.8	-0.7	--	--	--	--
G-26	3066.83	Carb&Eva	-6.4	-1.2	-28.4	-0.38	0.06	--
G-27	3067.50	Carb&Eva	-6.2	-3.5	--	--	--	--
G-28	3068.75	Carb&Eva	-8.7	-1.8	--	--	--	0.708530
G-29	3070.01	Carb&Eva	-11.5	-3	--	--	--	--
G-30	3071.39	Carb&Eva	-10.2	-0.8	-29.1	-0.50	0.05	--
G-31	3071.57	Carb&Eva	-3.1	-2.4	--	--	--	--
G-32	3073.07	Carb&Eva	-9.8	-3.9	--	--	--	--
G-33	3074.11	Carb&Eva	-9.1	-4.9	--	--	--	--
G-34	3075.33	Carb&Eva	-5.2	-1.2	-28.3	-0.76	0.08	0.708404
G-35	3075.56	Carb&Eva	-6.6	-3.3	--	-0.69	0.03	--
G-36	3077.08	Carb&Eva	-7.8	-3.6	--	--	--	--
G-37	3077.25	Carb&Eva	-7.5	-5.9	-28.0	-0.70	0.06	--
G-38	3078.38	Carb&Eva	-7.9	-1.2	--	--	--	--
G-39	3079.47	Carb&Eva	-9.8	-2.9	--	--	--	--
G-40	3080.12	Carb&Eva	-9.7	-5.5	-28.0	-0.63	0.04	--
G-41	3080.80	Carb&Eva	-8.3	-5.4	--	--	--	0.708373
G-42	3081.40	Carb&Eva	-10.7	-6.4	--	--	--	--
G-43	3082.46	Carb&Eva	-11.1	-6.1	-27.1	-0.49	0.06	--
G-44	3083.21	Carb&Eva	-12	-6.9	-27.0	-0.65	0.06	--
G-45	3085.42	Carb&Eva	-9.9	-6.7	-27.8	-0.71	0.06	--
G-46	3086.20	Carb&Eva	--	--	-27.3	--	--	--
G-47	3087.68	Carb&Eva	-8.2	-7.3	-27.9	-0.52	0.04	--
G-48	3089.84	Carb&Eva	-10.7	-7.2	-28.4	-0.48	0.05	--
G-49	3091.44	Carb&Eva	-11.3	-9.2	-27.9	-0.61	0.15	--
G-50	3091.80	Carb&Eva	-10.4	-4.2	-27.4	-0.42	0.04	--
G-51	3092.88	Carb&Eva	-10.4	-6.7	--	--	--	--
G-52	3093.37	Carb&Eva	-10.6	-5.8	--	--	--	0.708286
G-53	3094.66	Carb&Eva	-9.8	-4.1	--	-0.39	0.08	--
G-54	3097.23	Carb&Eva	-5.4	-3.6	--	--	--	--
G-55	3097.50	Carb&Eva	-5.6	-5	--	--	--	--
G-56	3098.98	Carb&Eva	-5.8	-4.5	-27.9	-0.42	0.04	--
G-57	3099.07	Carb&Eva	-7.4	-6	-27.4	-0.41	0.04	--
G-58	3099.50	Carb&Eva	-1	-2.5	--	--	--	--

G-59	3100.00	Carb&Eva	-7.8	-5.9	-28.1	-0.36	0.03	0.708336

-- data not measured or unavailable; carb: carbonate; Eva: evaporate

3. Modeling the C and U isotope values of authigenic carbonates

To provide a quantitative framework to interpret the C and U isotopic variations of the authigenic carbonates, we used a model with U reduction coupled with organic matter decomposition (modified from Zhao et al., 2016). The model also includes sulfate reduction and methanogenesis. The start of U reduction was assumed to have be synchronous with the onset of sulfate reduction. Dissolved inorganic carbon (DIC) and calcium were also included in the model to simulate the growth of authigenic carbonate.

The variation of geochemical compositions within the sedimentary profile at the seafloor was simulated using the following functions (Berner, 1980, Boudreau, 1997).

$$\frac{\partial C_l}{\partial t} = \frac{1}{\phi}\frac{\partial}{\partial x}\left(\phi D \frac{\partial C_l}{\partial x}\right) - \frac{1}{\phi}\frac{\partial}{\partial x}(\phi \upsilon C_l) + \sum R_l \qquad (1)$$

$$\frac{\partial C_s}{\partial t} = -\frac{1}{1-\phi}\frac{\partial}{\partial x}\left((1-\phi)\omega C_s\right) + \sum R_s \qquad (2)$$

Where Cl represents the concentration of a solute component, Cs represents concentration of a solid component, D represents the molecule diffusion, ϕ is porosity, υ represents the advection rate of pore water, ω represents the advection rate of sediments, R_s is the solid reaction rate, and R_l is the solute reaction rate. The effect of tortuosity on diffusion was included as $D = D_m/(1 - 2\ln\phi)$, of which the Dm is the molecule diffusion. The effects of compaction on υ and ω are also included. The modeled components, boundary conditions, parameters reaction functions and the reaction rate laws are listed in Table 1 to 5.

A continuum-type model (Boudreau and Ruddick, 1991) was used to describe organic matter degeneration.

$$\frac{\mathrm{dG}}{dt} = \frac{v}{a} \cdot \frac{G^{\frac{v+1}{v}}}{G_0^{\frac{1}{v}}} \qquad (3)$$

Where G is the organic matter, G0 is the initial concentration of organic matter, a represents the average life-time for the more reactive organic matter and v represents the shape of organic matter distribution. A Monod scheme was used for the reaction rate law of the main pathways for organic matter degeneration (Table 3).

The model domain has a thickness of 300 cm, which has 50 levels with their lengths gradually increasing from the top to the bottom of the model domain. The code was written in R language (R Development Core Team, 2006). The package ReacTran was used for the description of diffusion and advection (Soetaert and Herman, 2009). To solve the model, the method of line was applied. First, the original partial differential equations (PDEs) in the model were convert to the ordinary differential equations (ODEs). Then, a Variable Coefficient Ordinary Differential Equations (VODE) solver (Soetaert et al., 2010) was used to solved these ODEs.

Table S2.

Chemical species and boundary conditions of the model

Solids	**Value**	**Unit**	**notes**
organic carbon (G)	2.5-11	%	
U^{238} of sediments other than carbonates (SU^{238})	0	mmol cm^{-3}	
U^{235} of sediments other than carbonates (SU^{235})	0	mmol cm^{-3}	
Calcite	0	mmol cm^{-3}	
C^{13} of calcite	0	mmol cm^{-3}	

U^{238} of calcite	0	mmol cm^{-3}	
U^{235} of calcite	0	mmol cm^{-3}	
Solute			
Sulfate (SO_4^{2-})	30	mM	
Methane (CH_4)	0	mM	
U^{238} of pore water (LU^{238})	1.290633e-08	mmol cm^{-3}	
U^{235} of pore water (LU^{235})	9.366788e-11	mmol cm^{-3}	$d^{238}U$ = -0.39‰
DIC	2.5	mM	
C^{13} of DIC	2.778767e-02	mM	$d^{13}C$ =0‰
Ca	10	mM	

Note: the boundary conditions are for the upper boundary; while the conditions for the lower boundary were not set.

Table S3.

The reactions of the model

Number	reactions
R1	$CH_2O + O_2 \rightarrow CO_2 + H_2O$
R2	$CH_2O + \frac{1}{2}SO_4^{2-} + \frac{1}{2}H^+ \rightarrow CO_2 + \frac{1}{2}HS^- + H_2O$
R3	$CH_2O \rightarrow \frac{1}{2}CO_2 + \frac{1}{2}CH_4$
R4	$CH_2O + 2UO_2^{2+} + H_2O \rightarrow CO_2 + 2UO_2 + 4H^+$
R5	$SO_4^{2-} + CH_4 \rightarrow HS^- + H_2O + CO_3^{2-} + H^+$
R6	$Ca^{2+} + CO_3^{2-} \rightarrow$ Calcite

Table S4.

The laws of reaction rates

Number	laws
R1	$\frac{v}{a} \cdot \frac{G^{\frac{v+1}{v}}}{G_0^{\frac{1}{v}}}$
R2	$\frac{v}{a} \cdot \frac{G^{\frac{v+1}{v}}}{G_0^{\frac{1}{v}}} \cdot \left(\frac{[SO_4^{2-}]}{KSO_4 + [SO_4^{2-}]}\right)$
R3	$\frac{v}{a} \cdot \frac{G^{\frac{v+1}{v}}}{G_0^{\frac{1}{v}}} \cdot \left(\frac{KSO_4}{KSO_4 + [SO_4^{2-}]}\right)$

R4	$f_U \frac{v}{a} \cdot \frac{G^{\frac{v+1}{v}}}{G_0^{\frac{1}{v}}} \cdot (\frac{[U]}{KU + [U]})$	
R5	$K5 \cdot SO_4 \cdot CH_4$	
R6	$kcalc^+ \cdot (\Omega_{calc} - 1)$	$\Omega_{calc} > 1$
	$kcalc^- \cdot (\Omega_{calc} - 1) \cdot calc$	$\Omega_{calc} < 1$
Ω_{calc}	$([CO_3^{2-}] \cdot [Ca^{2+}])/Ksp_{calc}$	

Table S5.

The parameters of the model

symbol	description	Value	unit	Sources
L	The length of the model domain	300	cm	*
BW_temp	Bottom water temperature	12	^oC	*
BW_Sal	Bottom water salinity	35	‰	*
BW_Pr	Bottom water pressure	2	bar	*
BW_pH	Bottom water pH	7.40-7.43		*
ϕ	Porosity	0.8	1	*
ρ	The density of sediment	2.5	g cm^{-3}	*
ω_0	Sediment rate	0.01	cm yr^{-1}	*
a	Average life-time of the more reactive organic matter	4.5	yr	*
v	Shape of organic matter distribution	0.15	1	*
KSO_4	Limiting concentration of SO_4^{2-}	1.6	mM	a
KU	Limiting concentration of U in pore water	0.13	nM	*
	Isotopic fractionation during the reduction of U	1.0011	1	b
f_U	The rater of U reduction relative to sulfate reduction	$1*10^{-5}$	1	*
KD_U	Distribution coefficient of U in carbonate	1	1	c
$d^{13}Corg$	Carbon isotopes of organic carbon	-25	‰	*
K5	Rate constant of reaction 5	1e4	M^{-1} yr^{-1}	a
$kcalc^+$	Rate constant of calcite precipitation	1e-2	M yr^{-1}	*
$kcalc^-$	Rate constant of calcite dissolution	0.5	yr^{-1}	d
K1CO2	First dissociation constant of carbonate ion	1.096665e-06	M	e
K2CO2	Second dissociation constant of carbonate ion	6.792587e-10	M	e
Kspc	Apparent equilibrium constant of calc	4.551264e-07	M^2	e
DSO4	Diffusion coefficient of SO_4^{2-}	225.811	cm^2 yr^{-1}	f

DCH4	Diffusion coefficient of CH_4	389.0372	$cm^2\ yr^{-1}$	f
DHCO3	Diffusion coefficient of HCO_3^-	246.3178	$cm^2\ yr^{-1}$	f
DCO2	Diffusion coefficient of CO_2	404.1924	$cm^2\ yr^{-1}$	f
DCO3	Diffusion coefficient of CO_3^{2-}	197.9382	$cm^2\ yr^{-1}$	f
DCa	Diffusion coefficient of Ca^{2+}	169.3582	$cm^2\ yr^{-1}$	f
DUO2	Diffusion coefficient of UO_2^{2+}	67.21625	$cm^2\ yr^{-1}$	g

Note: the source of the parameters. a: Wang and Van Cappellen, (1996); b: Luff et al., 2004; c: Andersen et al. (2014); d: Zhao et al., 2015; e: calculated by package "seacarb"; f: calculated by package "marelac"; g: Li and Gregory, 1974; * this study.

References:

Andersen, M. B., Romaniello, S., Vance, D., Little, S. H., Herdman, R. & Lyons, T. W., 2014. A modern framework for the interpretation of $^{238}U/^{235}U$ in studies of ancient ocean redox. Earth and Planetary Science Letters, 400, 184-194

Berner, R. A., 1980. Early Diagenesis: A Theoretical Approach. (Princeton University Press).

Boudreau, B. P., , 1997. Diagenetic Models and Their Implementation: Modelling Transport and Reactions in Aquatic Sediments. (Springer-Verlag, Berlin).

Boudreau, B. P. & Ruddick, B. R., 1991. On a Reactive Continuum Representation of Organic-Matter Diagenesis. American Journal of Science, **291**, 507-538.

Li, Yuan-Hui, and Gregory, Sandra., 1974. Diffusion of ions in sea water and in deep-sea sediments. Geochimica et Cosmochimica Acta, 38, 5, 703-714.

Luff, R., Wallmann, K. & Aloisi, G., 2004. Numerical modeling of carbonate crust formation at cold vent sites: significance for fluid and methane budgets and chemosynthetic biological communities. Earth and Planetary Science Letters, 221, 337-353.

R development core team, 2006. R: A language and environment for statistical computing. R Foundation for Statistical Computing 61, 1673-1676.

Soetaert, K. & Herman, P. M. J., 2009. A practical guide to ecological modelling: Using R as a simulation platform. (Springer).

Soetaert, K., Petzoldt, T. & Setzer, R. W., 2010. Solving Differential Equations in R: Package deSolve. Journal of Statistical Software, 33, 1-25.

Wang, Y. F. & Van Cappellen, P., 1996. A multicomponent reactive transport model of early diagenesis: Application to redox cycling in coastal marine sediments. Geochimica et Cosmochimica Acta, 60, 2993-3014.

Zhao, M.Y., Zheng, Y.F., & Zhao, Y.Y., 2016. Seeking a geochemical identifier for authigenic carbonate. Nature Communications, 7, 1-7.

4. Figure S1

Carbon and oxygen isotope records of the carbonate from the studied Lower Middle Triassic Leikoupo interval display the similarity to the Neoproterozoic global Shuram excursion in terms of magnitude and asymmetry of $\delta^{13}C_{carb}$.

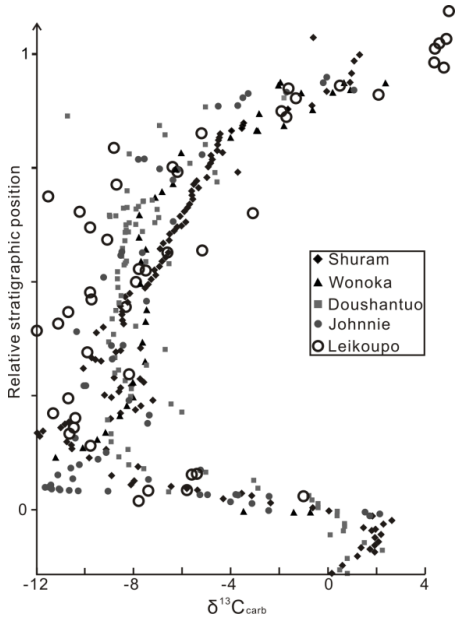

5. Figure S2

Paired carbon and oxygen isotopic compositions show strong correlation in authigentic dolomite in the studied Middle Triassic Leikoupo interval (A), as well as in carbonates from the Neoproterozoic Shuram excursions in Oman (B) (Fike et al., 2006), South China (C) (Jiang et al., 2007), and South Australia (D) (Calver, 2000). Also shown are relationships estimated by linear regression with 95% confidence intervals. Each of these panels shows data relationships that are statistically discordant with the predictions, with $p<0.0001$ and R^2 in a range of 0.53 to 0.91. VPDB—Vienna Peedee belemnite.

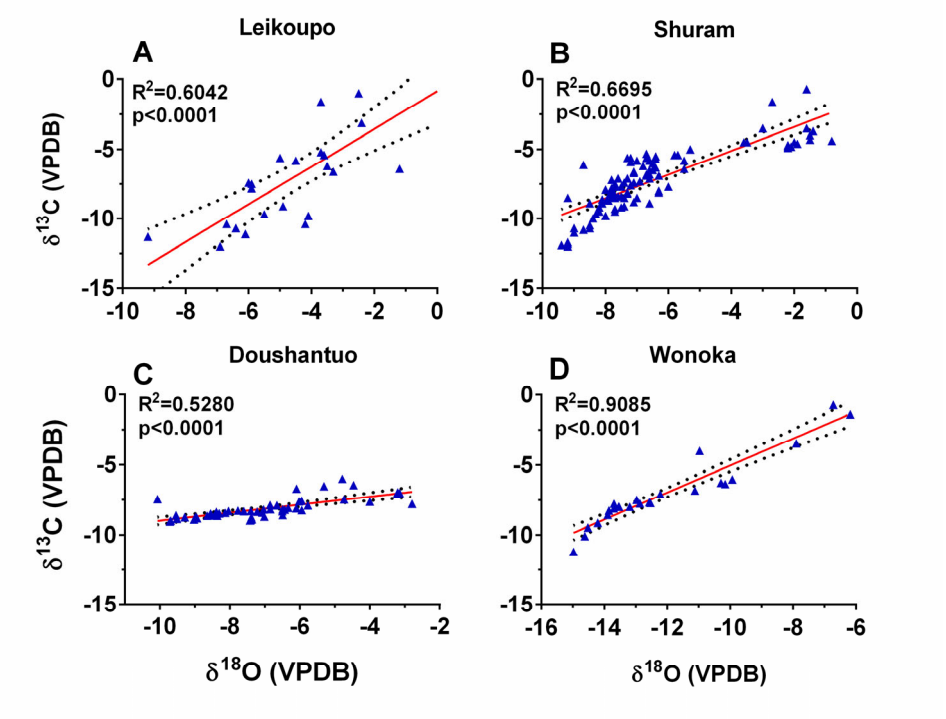

6. Figure S3

$\delta^{238}U$ and $\delta^{13}C$ modelling of authigenic carbonate. Note that almost all of the measured $\delta^{238}U$ and $\delta^{13}C$ values of carbonates located well within the modelling isotopic range under conditions ranging between 7.40 and 7.43 for pH, and an initial (sediment water interface) TOC value between 2.5% and 10%. See appendix for full model details.